A System for Monitoring Damage in Composite Materials Using Statistical Calibrations and Bayesian Model Selection

K. Ravi-Chandar, D. Faghihi, and J. T. Oden

Abstract This chapter summarizes the results of a feasibility study exploring the development of a stochastic Dynamic Data-Driven Application System (DDDAS) for prediction and monitoring of material damage in composite materials common to many types of contemporary high-performance military aircraft. The methodology involves (1) acquiring data from mechanical experiments conducted on a composite material; (2) the use of continuum damage mechanics based material constitutive models; (3) developing a Bayesian framework for uncertainty quantification, calibration, validation, and selection of models; and (4) general Bayesian filtering algorithm. The Bayesian framework, enables statistical calibration of the computational models of material damage against experimental observations, along with quantifying the inherent uncertainties in the data, the model, and the numerical solution approach. Moreover, the real-time monitoring of the damage evolution with the proposed approach results in enhancement of predictive models which allows forecasting failure in the structural components given the near real time experimental measurements.

K. Ravi-Chandar
Department of Aerospace Engineering and Engineering Mechanics, The University of Texas at Austin, Austin TX 78712 e-mail: ravi@utexas.edu

D. Faghihi
Institute for Computational Engineering and Sciences, The University of Texas at Austin, Austin TX 78712 e-mail: danial@ices.utexas.edu

J. T. Oden
Institute for Computational Engineering and Sciences, The University of Texas at Austin, Austin TX 78712 e-mail: oden@ices.utexas.edu

1 Introduction

The use of composite materials in the construction of next-generation aircraft has become a more frequent practice due to their high strength, relatively low weight, and corrosion resistance compared with similar structures made from metal, mainly aluminum and alloys. Durability and the resistance to cyclic stress or environmental degradation of these materials is a major factor in governing the require level of safety of the aerospace structures. Moreover, rate of damage growth and retaination of high level of residual strength in the presence of material damage is a critical issue in determining the frequency and cost of inspections and the need for repairs through the life of this type of aircraft. Therefore, it is very crucial to monitor and track the evolution of damage in structures composed of composite materials.

The Dynamic Data-Driven System (DDDAS) concept entails the use of experimental systems that deliver relevant data in near-real time to computational models of the evolution of physical phenomena of interest so as to allow feedback to control outputs to meet a set of objectives (see [1, 2, 3, 4, 5, 6, 7]). This study aims to develop a stochastic DDDAS for prediction and monitoring of material damage in composite materials such as are common in aircraft structures.

The physical problem under study is the experimental responds of thin composite structural components under loads that can generate distributed damage in the structure. Such measurements are subject to some uncertainty as a wide range of errors and inaccuracies can be involved in the experimental procedures. On the other hand, the computational models based on finite element solutions of continuum damage theories are used to model the onset and evolution of damage, generally in the form of micro-crack densities. These typically involve material parameters that exhibit uncertainties. A DDDAS is developed here that allows the quantification and measurement of uncertainties in experimental data, damage model parameters, and in the selection of the model itself, as well as modeling and potentially controlling the extent of damage accumulated in the laboratory experiments performed. In this regard, a Bayesian framework is adopted for defining, updating, and quantifying uncertainties in the model, the experimental data, and the target quantities of interest.

This chapter is structured as follows. A summary of basic concepts of continuum damage mechanics models is presented in Section 2. This is followed, in Section 3, by the development of a corresponding DDDAS. In Section 4, the experimental program is described. Section 5 is devoted to the computational algorithms needed in the system, including Bayesian model updating and general Bayesian filtering. Section 6 presents the experimental observations along with the results of calibration of damage model parameters, model plausibility, and monitoring the damage variable based on the experimental data. Summary and conclusions are outlined in Section 7.

2 Continuum Damage Mechanics

Structural components constructed using most engineering materials, either due to the manufacturing process or under the unfavorable conditions (e.g. mechanical loading, environmental conditions, and temperature variation) during their lifetime, may develop microscopic defects and cracks. The distribution of such defects are not only responsible for the macro-crack initiation and the final failure, but also for the induced deterioration or damage, such as a reduction in strength, rigidity, toughness, stability, and residual life.

The main objective of a damage theory is to model the evolution of damage, the loss of structural stiffness, over the lifetime of structural materials and determine the overall safety regimes in which the structure can function. Damage mechanics and fracture mechanics are both concerned with the behavior of the medium in order to estimate the safety and the serviceability of a structure, but in contrast to fracture mechanics, damage mechanics treats the material in such a way that the defects exist on a microscopic scale and they are continuously distributed within the material. Thus, the physical and mechanical properties of material depend on the distribution of such micro-cracks.

Kachanov [8] was the first to introduce continuous variables related to the density of the microscopic defects present in the material. These variables are subsequently embedded in the constitutive relationship of a damage state which may be employed in order to predict the initiation and growth of the micro-cracks. This concept has been formulated within the framework of thermodynamics and continuum mechanics. Therefore, compared to classical continuum mechanics, damage mechanics has the special characteristics such as: (1) A damage variable is introduced to represent the macroscopic effects of microscopic defects of material; (2) Damage kinetic (evolution) equation is postulated to describe the law of damage growth.

In the case where the damage variable does not depend on the orientation, the damaged state is characterized by a scalar field at a point $\mathbf{x}$ in a body at time t, $D = D(\mathbf{x},t)$), in which the value $D = 0$ characterizes the virgin (undamaged) state, while $D = D_c \leqslant 1$ characterizes the initiation of a macro-crack. The parameter D_c is a critical value for the damage variable usually taken between 0.2 and 0.8 for engineering materials (see the references in Lemaître and Chaboche [9]). Although the damage process is a thermodynamically irreversible process, the deformation due to damage itself can be completely recovered upon unloading. Thus, the recoverable part of the strain is attributed to cracks closure upon unloading and causes degradation in the material stiffness. In case of elastic-damage, the loss of elastic stiffness due to material damage is expressed the form of the reduced stress tensor,

$$\boldsymbol{\sigma} = (1-D)\,\mathbb{C}\,\boldsymbol{\varepsilon}, \tag{1}$$

where $\mathbb{C}$ is the fourth-order elastic tensor, $\boldsymbol{\sigma}$ is the second-oder stress tensor, and $\boldsymbol{\varepsilon}$ is the strain tensor.

Moreover, by postulating a proper form of energy dissipation due to material damage, one can write the following damage criterion (for more detail on the thermodynamic formulation of damage mechanic see [10]),

$$Y \leq \omega(\boldsymbol{\theta}, D), \tag{2}$$

where Y is the effective elastic energy density

$$Y = \boldsymbol{\varepsilon} : \mathbb{C}\boldsymbol{\varepsilon}, \tag{3}$$

and $\omega(\boldsymbol{\theta}, D)$ is the threshold of damage, for the particular damage model in use, which is function of the damage variable D and the materials parameters, represented in parameter vector $\boldsymbol{\theta}$.

As mentioned previously, the second characteristic of a continuum damage mechanic based formulation is an evolution equation for the damage variable to characterize the progression of degradation in the course of material deformation. Several evolution equations exist in the literature for damage variable (Table 1) that provide different forms of ω (i.e. damage models). For example, two simple damage models, proposed by Krajcinovic and Foneska [11] and Marigo [12], results in following function forms,

- Krajcinovic Damage Model:

$$\omega = \frac{1}{2} E \varepsilon_R^2 D^{\left(\frac{2}{s+1}\right)}, \tag{4}$$

- Marigo Damage Model:

$$\omega = \frac{1}{2} \frac{\beta^{2\alpha}}{E^{2\alpha - 1}} \ln\left(\frac{1}{1-D}\right). \tag{5}$$

Table 1 Various evolution equations for the damage variable.

Model	Damage Evolution	Model Parameters	Reference
M_1	$\dot{D} = (s+1)\frac{\varepsilon^s}{\varepsilon_{\mathrm{R}}^{(s+1)}}\dot{\varepsilon}$	$\boldsymbol{\theta}_1 = (E, \varepsilon_{\mathrm{R}}, s)$	Krajcinovic and Foneska [11]
M_2	$\dot{D} = \frac{2E^{2\alpha}(D-1)\varepsilon}{\beta^{\alpha}}\dot{\varepsilon}$	$\boldsymbol{\theta}_2 = (E, \alpha, \beta)$	Marigo [12]
M_3	$\dot{D} = \left[\frac{\sigma}{c_1(1-D)}\right]^{c_2}$	$\boldsymbol{\theta}_3 = (E, c_1, c_2)$	Kachanov [8]
M_4	$\dot{D} = c\varepsilon^{\alpha}\left[exp\left(-\frac{\beta}{T}\right)\right]\sigma^{\gamma}t^{\delta}$	$\boldsymbol{\theta}_4 = (E, c, \alpha, \beta, \gamma, \delta)$	Belloni et al. [13]

To complete the description of a mathematical model of damage in the elastic structure, quasi-static deformations of a material body occupying an open bounded domain $\Omega \subset \mathbb{R}^3$ with smooth boundary $\partial\Omega$ is considered. Hence, the initial boundary value model is defined by the following system,

$$\left.\begin{array}{rl} \nabla.\boldsymbol{\sigma}(\mathbf{x},t) = 0 & \forall\, \mathbf{x} \in \Omega, \\ \mathbf{u} = \mathbf{u}_0(\mathbf{x},t) & \forall\, \mathbf{x} \in \Gamma_u, \\ \boldsymbol{\sigma}\mathbf{n} = \mathbf{g}_0(\mathbf{x},t) & \forall\, \mathbf{x} \in \Gamma_\sigma, \end{array}\right\}, \tag{6}$$

where $\boldsymbol{\sigma}(\mathbf{x},t)$ is the Cauchy stress at point $\mathbf{x}$ on Ω at time t, $\mathbf{u}_0$ and $\mathbf{g}_0$ are prescribed displacement and tractions on surfaces $\Gamma_u \subset \partial\Omega$ and $\Gamma_\sigma \subset \partial\Omega$ respectively, and $\mathbf{n}$ denotes the outward unit normal to $\partial\Omega$. The above governing equation is solved numerically using Finite Element Method, with $t \in [0,T)$. In this regard, the stress state evaluation is achieved by discretizing the evolution equations of the stress and damage together with the consistency conditions,

$$Y\left(\mathbf{x},t^{(k+1)}\right) - \omega\left(\theta, D\left(\mathbf{x},t^{(k+1)}\right)\right) \leq 0. \tag{7}$$

To insure the above consistency conditions, an implicit Backward Euler method is utilized here. In this regard, the incremental value of the damage variable can be obtained using the Newton iterative procedure (see [10] for more details).

3 The Dynamic Data Driven Application System

The physical problem under study is the evolution of damage in polymer nanocomposite material that is commonly used in aerospace applications. The laboratory manufactured specimen is subjected to a monotonically increasing load or load-unload cycles with increasing load up to failure. At different stages in this process, the specimen is examined in order to determine the spatial variation in the strain using digital image correlation and map this to damage. Moreover, the computational models based on finite element solutions of the continuum damage theories are taken into account to model the initiation and growth of damage.

Figure 1 shows that how the DDDAS connects the aforementioned experimental measurements with the computational model. In this figure "state" means a joint probability density function (PDF) of the material parameters and the damage field throughout the specimen. There are two main computational cycles can be observed from this figure. Starting with an initial state (i.e. no damage), the computational model is exercised during the solution of the statistical forward problem for one time step. While experimental data is not available, the predicted state feeds back through the statistical forward problem, so that the state can be predicted at the next time step. The other computational cycle in Figure 1 involves a Bayesian updating procedure, and is responsible for dynamically updating our knowledge about the state, as data is collected. Once experimental data is accessed at a particular time, one can use it to update our knowledge about the system state, using prior knowledge (predicted state) to gain posterior knowledge (corrected state). The computational model and the experimental data are used in the computation of the likelihood function in Bayes formula (see Section 5). The corrected damage state is then fed back to the forward problem as one advances in time and the loop begins again.

In order to more accurate prediction of the state, the finite element mesh may need to be refined. The corrected damage state might also drive other control actions, as indicated by the three dotted lines on the bottom of Figure 1. For instance, in cases in which the material is part of an airplane in service, possible actions (i.e. control) might be:

- to instantly apply healing[1] to a damaged region;
- to instantly update a flight maneuver plan in order to diminish the possibility that any further damage happens to the system;
- update the flight computer so that it has up-to-date information before taking a maneuver decision.

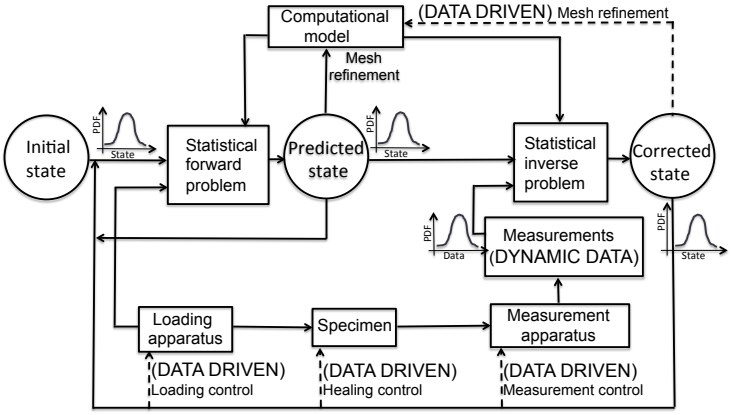

Fig. 1 A schematic representation of the DDDAS developed in this study. The four dotted lines highlight the possible (dynamic) data driven actions.

As will be mentioned later in this chapter many uncertainties are involved in the process of assessing the system state, such as noise in experimental data and model inadequacy. All these uncertainties justify the use of statistical problems in Figure 1.

4 Experiments

In order to provide experimental evidence for conducting statistical calibration, validation and selection of the continuum damage models, a set of experimental data are dynamically recorded for a polymer nano-composite material. Details regarding the manufacturing process of the specimen can be found in [10]. The experimental work

[1] Healing refers to the activation of another mechanism that locally reduces damage by recovering local stiffness of the material.

involves uniaxial tensile experiments with different load levels for measuring strain variation over the length of the specimens, and for generating distributed damage in different parts of the specimen. Moreover, in order to provide for real-time monitoring of damage, [10] postulated a second group of experiments for dynamically and indirect measuring local variation of damage along the length of the specimen.

The specimens are made of a bisphenol A epoxy resin infused with multiwalled carbon nanotubes (CNTs) dispersed uniformly through the specimen. The presence of the CNTs makes the specimen electrically conductive and provides the possibility of determining the damage state through electrical conductivity measurements. These specimens are subjected to loading-unloading cycles with progressively increasing peak displacements between two rigid cross-heads in a testing machine. The global response of the specimen is characterized easily by measuring the force and extension. The spatial variation in the strain field (resulting from local perturbations in material state and properties) is also measured at each load increment using digital image correlation. Moreover, the spatial variation of electrical conductivity (averaged across the width of the specimen) is measured using a four-point conductivity probe at a selected number of positions along the length of the specimen. The connection between the conductivity changes and damage in term of microcracks can provide an indirect measurement of damage. However, observations of [10] suggest that the underlying mechanisms that dictate the changes in resistance with position, strain and stress, as well as time-dependence are quite complex and may require a more in-depth examination before the CNT infiltrated epoxies can be used as diagnostic sensors. Therefore, in the current work, the results of the indirect measurement of damage is not considered for the statistical analyses.

Uniaxial tensile loading, interspersed with loading-unloading cycles, are performed on rectangular strip specimens. The global response of the specimen is characterized easily by measuring the force and extension. The spatial variation in the strain field (resulting from local perturbations in material state and properties) is measured at each load increment using digital image correlation. In this method of strain measurement, the specimen is covered with a fine speckled pattern applied by spray-painting. This speckle pattern is then imaged at high spatial resolution at each load increment. By comparing the speckle pattern in the initial and deformed specimen through a cross-correlation procedure, the displacement of each point within the specimen is identified, and the strain is then calculated.

5 Bayesian Analyses and Model Plausibilities

5.1 Bayesian Model Calibration

In order to make predictions about the failure of the system and consequently be informed the prototype of potential control actions to be taken, the continuum damage mechanics model (i.e. mathematical model) of Section 2 needs to be calibrated

against the test results. Calibration processes, by definition, involve determining model parameters to best fit experimental data. However, many uncertainties are involved in the process of assessing the predictability of mathematical and computational models of the physical event:

- the data is measured only at some points of the system;
- the measured data has noise;
- the continuum damage mechanic models are, at best, abstraction of reality and do not capture real responses of the material perfectly;

In order to quantify such uncertainties in the calibrated model parameters, statistical inverse theory is employed. Such statistical calibration involves statistically inferring the set of physical parameter values, indicated by the vector $\boldsymbol{\theta} \in \mathbb{R}^{n_\theta}$ (i.e. material constants of the damage models), using the measurement data $\mathbf{d} \in \mathbb{R}^{n_d}$ (i.e. strain measurements). The pre-inference and uncertain knowledge of the model parameters is represented by the prior probability density function $\pi_{\text{prior}}(\boldsymbol{\theta})$. The posterior (post-inference) state is given by Bayes' formula [14]:

$$\pi_{\text{post}}(\boldsymbol{\theta}|\mathbf{d}) = \frac{\pi_{\text{like}}(\mathbf{d}|\boldsymbol{\theta}) \cdot \pi_{\text{prior}}(\boldsymbol{\theta})}{\pi_{\text{data}}(\mathbf{d})}. \tag{8}$$

In (8), $\pi_{\text{post}}(\boldsymbol{\theta}|\mathbf{d})$ is the posterior PDF defining the Bayesian update of the prior information embodied in $\pi_{\text{prior}}(\boldsymbol{\theta})$. The assumptions regarding the discrepancy between the measured data and computed results are encapsulated in the likelihood PDF, $\pi_{\text{like}}(\mathbf{d}|\boldsymbol{\theta})$. Moreover, the marginalized PDF,

$$\pi_{\text{data}}(\mathbf{d}) = \int \pi_{\text{like}}(\mathbf{d}|\boldsymbol{\theta}) \cdot \pi_{\text{prior}}(\boldsymbol{\theta})\, d\boldsymbol{\theta}, \tag{9}$$

is called the "model evidence" and is affects the normalization constant making the posterior a PDF.

5.2 Model Plausibilities

The Bayesian methodology can be also used to the determination of the most plausible continuum damage model between two candidate models M_1 (=Krajcinovic damage model) and M_2 (=Marigo damage model), in order to simulate the measured data set $\mathbf{d}(t^{(k)}, x_i) = \left\{ u(t^{(t)}, x_i), f_{\text{exp}}(t^{(k)}) \right\}$. To make explicit the entire set of assumptions underlying the modeling and inference efforts, formula (8) can be rewritten [15, 16, 17],

$$\pi_{\text{post}}(\boldsymbol{\theta_j}|\mathbf{d}, M_j) = \frac{\pi_{\text{like}}(\mathbf{d}|\boldsymbol{\theta_j}, M_j) \cdot \pi_{\text{prior}}(\boldsymbol{\theta_j}|M_j)}{\pi_{\text{data}}(\mathbf{d}|M_j)}. \tag{10}$$

where M_j denotes the j-th model class, which has associated with it a random vector $\boldsymbol{\theta_j}$ of model parameters, $j = 1, 2, \ldots, m$. All m proposed model classes are "competing" to explain (match) the same collected data $\mathbf{d}$. That is, a model class can be seen as the family of all possible values of $\boldsymbol{\theta_j}$, augmented with prior and likelihood PDFs.

The model evidence (9) is now written as conditioned on the model,

$$\pi_{\text{data}}(\mathbf{d}|M_j) = \int \pi_{\text{like}}(\mathbf{d}|\boldsymbol{\theta_j}, M_j) \cdot \pi_{\text{prior}}(\boldsymbol{\theta_j}|M_j)\, d\boldsymbol{\theta_j}. \tag{11}$$

The model evidence can be used to update the ranking of model classes. Particularly, in the set $\mathscr{M} = \{M_1, \ldots, M_m\}$ of competing model classes, one can consider a priori plausibility $\rho_{\text{prior}}(M_j|\mathscr{M})$ for each model class, with the constraint $\sum_{j=1}^{m} \rho_{\text{prior}}(M_j|\mathscr{M}) = 1$.

Once new data is collected, one can update such a priori ranking. The posterior plausibility $\rho_{\text{post}}(M_j|\mathbf{d}, \mathscr{M})$ for each model class is also computed through a Bayesian updating procedure,

$$\rho_{\text{post}}(M_j|\mathbf{d}, \mathscr{M}) = \frac{\pi_{\text{data}}(\mathbf{d}|M_j, \mathscr{M}) \cdot \rho_{\text{prior}}(M_j|\mathscr{M})}{\pi_{\text{data}}(\mathbf{d}|\mathscr{M})}. \tag{12}$$

In (12), the term

$$\pi_{\text{data}}(\mathbf{d}|\mathscr{M}) = \sum_{j=1}^{m} \pi_{\text{data}}(\mathbf{d}|M_j, \mathscr{M}) \cdot \rho_{\text{prior}}(M_j|\mathscr{M}) \tag{13}$$

is the normalization value (for a given $\mathbf{d}$) that makes (12) a probability mass function (PMF)[2]. It reflects how likely one is to obtain a given data sample $\mathbf{d}$ with the whole family of model classes M_j in $\mathscr{M}$.

In this work, (10) and (12) are used in order to calibrate the Krajcinovic and Marigo damage models (see Table 1).

5.3 The General Bayesian Filtering

The real-time monitoring of the system state (e.g. scalar damage field throughout a volume region) requires the statistical evaluation of the system state evolution with time $t \in [0, +\infty)$, so the potential decisions and control actions can be taken about the system. The initial state of the system is specified by the PDF $\pi(\boldsymbol{\theta}^{(0)})$. The (eventual) control will be indicated by the vector $\mathbf{c} \in \mathbb{R}^{n_c}$, for some fixed positive integer $n_c > 0$. In order to assess the damage variable, Bayes' formula can be applied for the collect measurement data $\mathbf{d}^{(1)}$, $\mathbf{d}^{(2)}, \ldots$, at instants $0 = t^{(0)} < t^{(1)} < t^{(2)} < \ldots$, such as

$$\pi_{\text{post}}(\boldsymbol{\theta}^{(k)}|\mathbf{d}^{(k)}) = \frac{\pi_{\text{like}}(\mathbf{d}^{(k)}|\boldsymbol{\theta}^{(k)}) \cdot \pi_{\text{prior}}(\boldsymbol{\theta}^{(k)})}{\pi_{\text{data}}(\mathbf{d}^{(k)})}. \tag{14}$$

[2] note the use of "ρ" instead of "π".

In cases where control is applied or unpreventable events affects the state evolution, a Bayes filter can be constructed as a two step process,

(a) [Prediction step] An evolution equation is used to predict the state of the system. A possible discrete form of such evolution equation is

$$\boldsymbol{\theta}^{(k+1)} = \mathbf{f}^{(k+1)}(\boldsymbol{\theta}^{(k)}, \mathbf{c}^{(k+1)}, \mathbf{w}^{(k)}), \tag{15}$$

where $\mathbf{f}^{(k+1)}(\cdot,\cdot,\cdot)$ is an evolution function and $\mathbf{w}$ denotes the state noise. Once the new state $\boldsymbol{\theta}^{(k+1)}$ is predicted, one can also predict the next measurement to be obtained at $t^{(k+1)}$. A possible discrete form of such prediction is given by the output equation

$$\mathbf{y}^{(k+1)} = \mathbf{g}^{(k+1)}(\boldsymbol{\theta}^{(k+1)}, \mathbf{v}^{(k+1)}), \tag{16}$$

where $\mathbf{g}^{(k+1)}(\cdot,\cdot)$ is an output function and $\mathbf{v}$ denotes the output noise;

(b) [Correction step] Then, finally, one can actually measure data $\mathbf{d}^{(k+1)}$ at $t^{(k+1)}$. The comparison between the model output $\mathbf{y}^{(k+1)}$ and the measurements $\mathbf{d}^{(k+1)}$ in the likelihood PDF will then allow one to statistically update the predicted state $\boldsymbol{\theta}^{(k+1)}$ using Bayes' formula (14).

The steps (a)-(b) are repeated to continue assessing and controlling the state system. Such an updating process can be represented by the equation,

$$\pi_{\text{post}}(\boldsymbol{\theta}^{(k+1)}|\mathbf{d}^{(k+1)}, \mathbf{d}^{(k)}, \ldots, \mathbf{d}^{(1)}) = \frac{\pi_{\text{like}}(\mathbf{d}^{(k+1)}, \mathbf{d}^{(k)}, \ldots, \mathbf{d}^{(1)}|\boldsymbol{\theta}^{(k+1)}) \cdot \pi_{\text{prior}}(\boldsymbol{\theta}^{(k+1)})}{\pi_{\text{data}}(\mathbf{d}^{(k+1)}, \mathbf{d}^{(k)}, \ldots, \mathbf{d}^{(1)})}. \tag{17}$$

If one assumes (i) that the system state follows a first-order Markov process and (ii) given a current state, the measurements are independent of previous measurements, then (17) can be rewritten as [18, 19, 20]

$$\pi_{\text{post}}(\boldsymbol{\theta}^{(k+1)}|\mathbf{d}^{(k+1)}, \mathbf{d}^{(k)}, \ldots, \mathbf{d}^{(1)}) = \frac{\pi_{\text{like}}(\mathbf{d}^{(k+1)}|\boldsymbol{\theta}^{(k+1)}) \cdot \pi_{\text{prior}}(\boldsymbol{\theta}^{(k+1)}|\mathbf{d}^{(k)}, \ldots, \mathbf{d}^{(1)})}{\pi_{\text{data}}(\mathbf{d}^{(k+1)}|\mathbf{d}^{(k)}, \ldots, \mathbf{d}^{(1)})}. \tag{18}$$

In (18), the term

$$\pi_{\text{prior}}(\boldsymbol{\theta}^{(k+1)}|\mathbf{d}^{(k)}, \ldots, \mathbf{d}^{(1)}) = \int \pi_{\text{state}}(\boldsymbol{\theta}^{(k+1)}|\boldsymbol{\theta}^{(k)}, \mathbf{d}^{(k)}, \ldots, \mathbf{d}^{(1)}) \cdot \pi_{\text{post}}(\boldsymbol{\theta}^{(k)}|\mathbf{d}^{(k)}, \ldots, \mathbf{d}^{(1)})\, d\boldsymbol{\theta}^{(k)} \tag{19}$$

involves the evolution Equation (15), while the term $\pi_{\text{like}}(\mathbf{d}^{(k+1)}|\boldsymbol{\theta}^{(k+1)})$ involves the output Equation (16). The Bayesian filtering procedure (18) is usually intractable computationally. However, it can be simplified with further assumptions. For example, the case in which the system state is Gaussian, one possible approach is to linearize both the evolution function $\mathbf{f}^{(k+1)}(\cdot,\cdot,\cdot)$ in (15) and the output function $\mathbf{g}^{(k+1)}(\cdot,\cdot)$ in (16). In this regard, the aforementioned Bayesian filtering procedure can be reduced into the Extended Kalman filter. The general process (18) can then be substituted by the following five steps (Figure 2):

$$\tilde{\boldsymbol{\theta}}^{(k+1)} = \mathbf{f}^{(k+1)}(\hat{\boldsymbol{\theta}}^{(k)}, \mathbf{u}^{(k+1)}, \mathbf{0}), \tag{20}$$

$$\tilde{\mathbf{P}}^{(k+1)} = \mathbf{A}^{(k+1)} \cdot \mathbf{P}^{(k)} \cdot \mathbf{A}^{(k+1)^T} + \mathbf{W}^{(k+1)} \cdot \mathbf{Q}^{(k)} \cdot \mathbf{W}^{(k+1)^T}, \tag{21}$$

$$\mathbf{K}^{(k+1)} = \tilde{\mathbf{P}}^{(k+1)} \cdot \mathbf{H}^{(k+1)^T} \cdot \left(\mathbf{H}^{(k+1)} \cdot \tilde{\mathbf{P}}^{(k+1)} \cdot \mathbf{H}^{(k+1)^T} + \mathbf{V}^{(k+1)} \cdot \mathbf{R}^{(k+1)} \cdot \mathbf{V}^{(k+1)^T}\right)^{-1}, \tag{22}$$

$$\hat{\boldsymbol{\theta}}^{(k+1)} = \tilde{\boldsymbol{\theta}}^{(k+1)} + \mathbf{K}^{(k+1)} \cdot \left(\mathbf{d}^{(k+1)} - \mathbf{g}^{(k+1)}(\tilde{\boldsymbol{\theta}}^{(k+1)}, \mathbf{0})\right), \text{ and} \tag{23}$$

$$\hat{\mathbf{P}}^{(k+1)} = \left(\mathbf{I} - \mathbf{K}^{(k+1)} \cdot \mathbf{H}^{(k+1)}\right) \cdot \tilde{\mathbf{P}}^{(k+1)}, \tag{24}$$

where

$$\mathbf{A}_{ij}^{(k+1)} = \frac{\partial \mathbf{f}_i^{(k+1)}}{\partial \theta_j}(\hat{\boldsymbol{\theta}}^{(k)}, \mathbf{u}^{(k+1)}, \mathbf{0}), \tag{25}$$

$$\mathbf{W}_{ij}^{(k+1)} = \frac{\partial \mathbf{f}_i^{(k+1)}}{\partial w_j}(\hat{\boldsymbol{\theta}}^{(k)}, \mathbf{u}^{(k+1)}, \mathbf{0}), \tag{26}$$

$$\mathbf{H}_{ij}^{(k+1)} = \frac{\partial \mathbf{g}_i^{(k+1)}}{\partial \theta_j}(\tilde{\boldsymbol{\theta}}^{(k+1)}, \mathbf{0}), \tag{27}$$

and

$$\mathbf{V}_{ij}^{(k+1)} = \frac{\partial \mathbf{g}_i^{(k+1)}}{\partial v_j}(\tilde{\boldsymbol{\theta}}^{(k+1)}, \mathbf{0}). \tag{28}$$

Hence, it is assumed that one knows $\hat{\boldsymbol{\theta}}^{(0)}$, $\mathbf{P}^{(0)}$, $\mathbf{Q}^{(k)}$, and $\mathbf{R}^{(k+1)}$, $\forall\, k \geqslant 0$.

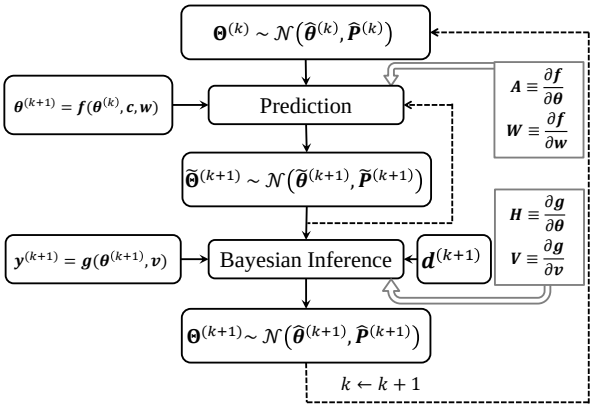

Fig. 2 Extended Kalman filtering algorithm.

6 Results

6.1 Experimental Observations

Figures 3 and 4 show the outcomes of the experiment conducted on CNT-Epoxy specimens and employed for the statistical calibration of the damage models. The overall elongation $\Delta^k = \left| u(t^{(k)}, x_N) - u(t^{(k)}, x_0) \right|$ between the ends of the specimen and the corresponding overall load on the specimen as measured by the load cell is shown in Figures 3. The results of this figure corresponds to the data $f_{\exp}(t^{(k)})$.

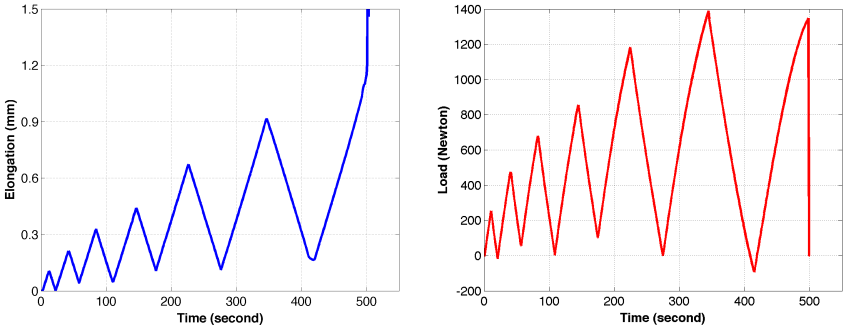

(a) (b)

Fig. 3 Experimental results of the CNT-Epoxy specimen (applied displacement rate = $0.025(mm.s^{-1})$): (a) displacement variation with time measured by DIC; (b) load variation with time measured by the load cell [10].

The progression of damage in the specimen can be inferred by considering the variation of the overall specimen displacement Δ^k and load $f_{\exp}(t^{(k)})$ as indicated in Figure 4(a); the nonlinearity experienced at strain levels greater than about 0.5% is an indication of inelastic response of the material that can be correlated to plasticity and/or damage. Figure 4(b) shows a contour plot corresponding to the strain, ε at a particular step in the loading process when the average strain in the specimen was about 1.4%. Figure 4(c) indicates the variation along x, the horizontal direction, of the strain at different times after beginning of the test (particularly at one set of each unloading). This data corresponds to $u(t^{(k)}, x_i)$, the measured displacement variation along x at time (i.e. load increment) k. There are two key features that are evident; first, while the average strain is about 1.4%, there is a background fluctuation over the entire length that arises from the noise in the process of digital image correlation used to evaluate the strains. Second, there are some hot-spots where the strains are quite a bit higher than the average strain; these fluctuations are well above the noise in the measurements and correspond to points in the specimen where local defects trigger damage accumulation. Eventually, one of these hot-spots results in failure of the specimen. This development of strain (or damage) accumulation is illustrated

in Figure 4(d) where the variation of the strain in the uniform segment is shown in comparison to the strain in the hot-spot; rapid accumulation of strain leading up to failure of the specimen occurs in the last cycle.

The measured displacement data $u(t^{(k)},x_i)$, and the corresponding measured force $f_{\exp}(t^{(k)})$ from the lead cell for all time steps, constitutes the experimental data set $\mathbf{d}(t^{(k)},x_i) = \left\{u(t^{(k)},x_i), f_{\exp}(t^{(k)})\right\}$ to be used in calibration of the damage model.

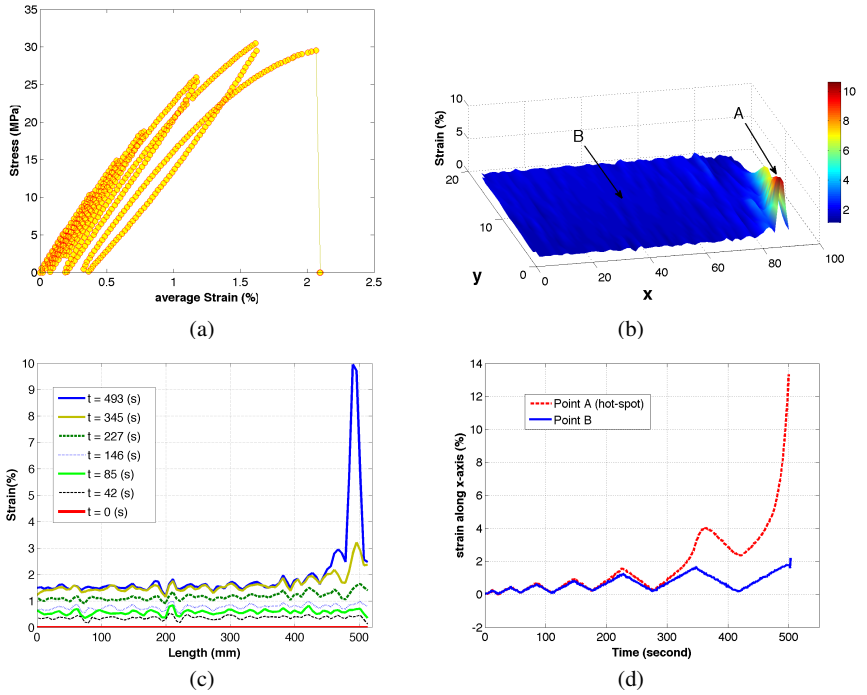

Fig. 4 Experimental results of the CNT-Epoxy specimen: (a) The nominal stress vs nominal strain plot indicating the load-unload cycles that the specimen experienced; (b) Spatial variation of strain at $t = 493$(s) after beginning the test; (c) the strain variation along x (line C as shown in plot (b)) at different times (one set of unloading); (d) evolution of strain through time in the hot-spot and in the uniform segment (points A and B as shown in plot (b) respectively)[10].

6.2 Statistical Calibration and Plausibility of Damage Models

In order to conduct the calibration and compute the evidences using the Krajcinovic damage model M_1 and the Marigo damage model M_2, one has to decide on the prior PDFs to be use for the random parameters as well as the form of likelihood. In the

absence of any prior information on parameters, but for specification of a finite set of possible values, it is customary to employ uniform priors, presenting complete ignorance, in which parameters values fall in intervals possibly suggested by experimental data (e.g. Figure 4(a)). Therefore, a uniform prior PDF for the material parameters is assumed here such that

$$\mathscr{U}\left((0.5e9,0.5e10)\times(-1,10)\times(0.001,1)\right) \text{ for } (E,s,\varepsilon_R), \tag{29}$$

and

$$\mathscr{U}\left((0.5e9,0.5e10)\times(0.001,5)\times(0.5e8,3e8)\right) \text{ for } (E,\alpha,\beta), \tag{30}$$

for M_1 and M_2 respectively. Here $\mathscr{U}(B)$ stands for a uniform distribution over a given set B.

6.2.1 The likelihood

It is known that in general the measurements $\mathbf{d}(t^{(k)},x_i)=\left\{u(t^{(k)},x_i),f_{\exp}(t^{(k)})\right\}$ do not agree with the actual physical entities due to presence of noise (i.e. error in data). Moreover, there is difference between the real values of the physical entities and those delivered by the continuum damage models (i.e. model inadequacy). The form of the likelihood function reflects the way the discrepancy between the quantities computed with the material constitutive relation and the reference data is modeled. Here it is assumed that the error in data and model are Gaussian random variables of mean $\mathbf{0}_{N_t\times 1}$ and (unknown) variances $\sigma^2_{\text{data(displ)}}\cdot\mathbf{I}_{N_tN_x\times N_tN_x}$ and $\sigma^2_{\text{data(load)}}\cdot\mathbf{I}_{N_t\times N_t}$, where N_t is the number of time steps and N_x is the number of position along x. Therefore one can construct the likelihood function of [21],

$$\begin{aligned}\ln(\pi_{\text{like}}(\mathbf{d}|\theta_j,M_j)) = \frac{1}{2}\ln(2\pi) - N_t\ln(\sigma_{\text{load}}) - N_tN_x\ln(\sigma_{\text{displ}}) + \\ -\frac{1}{2}\sum_{k=1}^{N_t}\left\{\left[\frac{f_{\exp}(t^{(k)})-f_{\text{model}}(\theta_j;t^{(k)})}{\sigma_{\text{load}}}\right]^2 + \right. \\ \left. +\sum_{i=1}^{N_x}\left[\frac{u_{\exp}(t^{(k)},x_i)-u_{\text{model}}(\theta_j;t^{(k)},x_i)}{\sigma_{\text{displ}}}\right]^2\right\},\end{aligned} \tag{31}$$

In addition to the physical parameters of the damage models, two random variables – so called (hyper) parameters – (σ_{displ} and σ_{load}) are involved in the statistical calibration process. These parameters can be interpreted as a measure of the overall discrepancy between the measured load and displacement and the corresponding quantities computed with the damage models.

6.2.2 Numerical results

The results of the statistical calibration the material parameters for the Marigo, $\boldsymbol{\theta} = (E, \alpha, \beta; \sigma_{\text{displ}}, \sigma_{\text{load}})$, damage models are presented in Figure 5 in term of posterior marginal kernel density estimation (KDE) of each parameter (see [21] for the results of calibration of the Krajcinovic damage model parameters). As indicated in Section 5, (12) provides the means to compare model class, M_j for the given set $\mathbf{d}$ of reference data and to pick the most plausible one. A model M_1 is believed to be superior over M_2 if $\rho_{\text{posterior}}(M_1|\mathbf{d}, \mathscr{M}) > \rho_{\text{posterior}}(M_2|\mathbf{d}, \mathscr{M})$. As denoted by the conditional notation, such model ranking depends upon the specific collected data. Moreover the model evidence π_{data} plays the fundamental role in ranking of model classes. An equal prior plausibility $\pi_{\text{prior}}(M_j|\mathscr{M}) = \frac{1}{2}$ is picked here for each damage model. Using this prior plausibility, the computed evidences and posterior plausibility are shown in Table 2. The computed values indicate that for the given

Table 2 Numerical results on log evidence and plausibilities (see (12)). One should note that ρ_{prior} and $\rho_{\text{posterior}}$ are probability mass function (PMF) [21].

Model	Log Evidence $\ln(\pi_{\text{data}}(\mathbf{d}\|M_j))$	Prior Plausibility $\rho_{\text{prior}}(M_j\|\mathscr{M})$	Posterior Plausibility $\rho_{\text{posterior}}(M_j\|\mathbf{d}, \mathscr{M})$
M_1:Krajcinovic Damage Model	4024.9	1/2	$\approx 1/2$
M_2:Marigo Damage Model	4025.49	1/2	$\approx 1/2$

set of reference data, both posterior plausibilities are practically equal to 50%, assuming prior plausibilities of 50%. This means that none of the selected damage models is superior over another in simulating the measured data. This is mainly due to the inadequacy of the provided information about the system. In other words, using only a basically uni-axial set of stress-strain as the set of reference data, will not supply enough evidence in order to differentiate between these two damage models. It should be noted that the main purpose of such calculation is to prove the feasibility of the developed framework for Bayesian model selection using the notion of model plausibility.

6.3 State Monitoring with Extended Kalman Filter

In order to statistically evaluate how the damage state develops in the material through time, the Extended Kalman Filter is applied on the damage models. In this regard, the material parameters of the damage models is fixed with the Maximum a Posterior (MAP) Estimation[3] values obtained from the statistical calibration results

[3] MAP for $\boldsymbol{\theta}$ is defined as $\hat{\boldsymbol{\theta}} = \arg\max_{\boldsymbol{\theta}} \pi_{\text{post}}(\boldsymbol{\theta})$

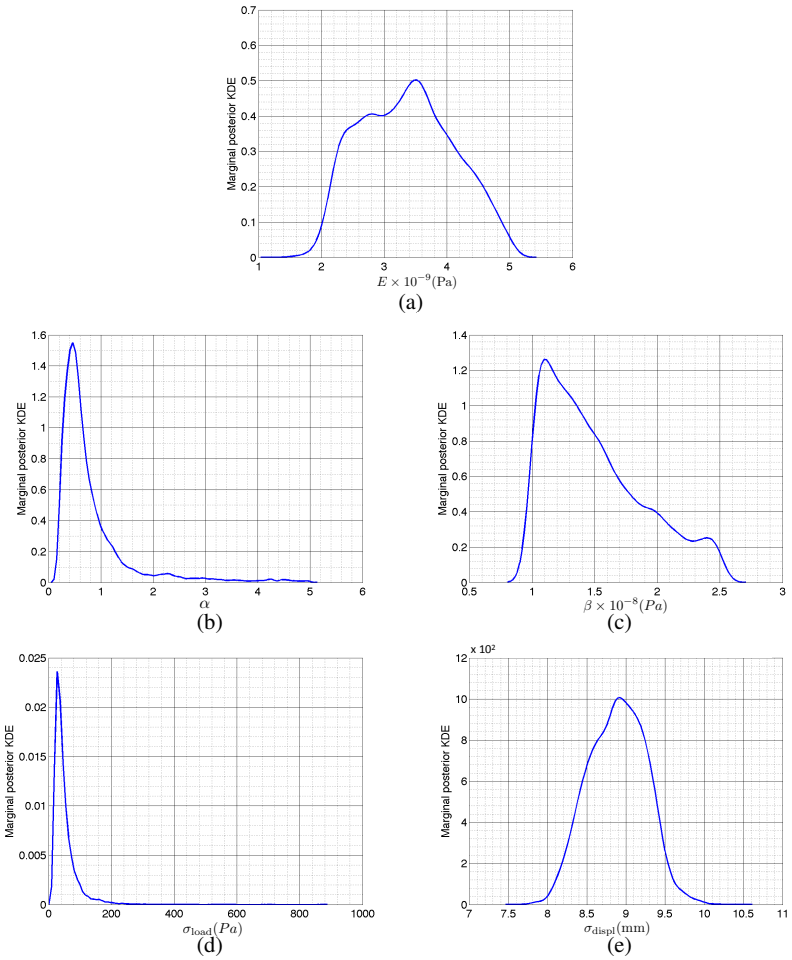

Fig. 5 Calibrated material parameters for Marigo damage model. Posterior marginal density estimation of (a) Elastic modulus E; (b) parameter α; (c) parameter β; (d) σ_{load}; and (e) σ_{disp} [21].

and filtering process is conducted on the damage variable, D, throughout the finite element mesh. Figures 6 and 7 show the results of the filtering the damage variables using the Marigo damage model and the experimental data in term of spatial and temporal variation of the damage mean vector and covariance matrix (see [21] for the results of filtering using the Krajcinovic damage model). The accumulation of damage during loading and unchanged value of the damage variable throughout the set of elastic unloading and reloading can be observed from these figures. Moreover, the results presented in Figure 6 indicate the higher rate of damage growth (material degradation) at the initial stage of the test in the *position id 1*. As indicated in Figure 4, this is the location of the observed *hot spot* in the experiment leading to

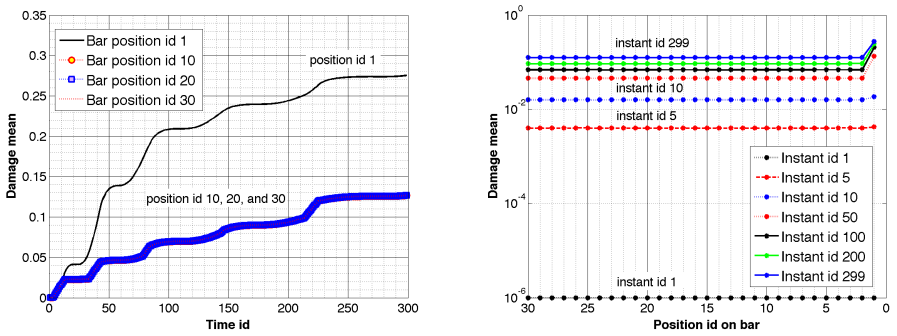

(a) (b)

Fig. 6 Evolution of damage mean vector for Marigo damage model with respect to (a) time $t^{(k)}$; (b) position x_i; using the fixed damage model parameters $E = 1 \times 10^9$(Pa) , $\alpha = 0.95$, and $\beta = 1 \times 10^8$(Pa) [21].

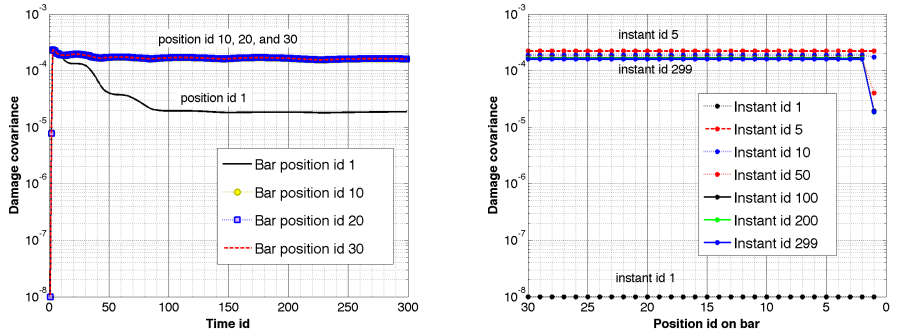

(a) (b)

Fig. 7 Evolution of damage covariance matrix for Marigo damage model with respect to (a) time $t^{(k)}$; (b) position x_i; using the fixed damage model parameters $E = 1 \times 10^9$(Pa) , $\alpha = 0.95$, and $\beta = 1 \times 10^8$(Pa) [21].

the material failure. Therefore the developed DDDAS infrastructure enables one to forecast the failure in the system given the near "real" time data, so that one can be informed for potential decisions to be taken about the system, and/or for potential control actions to be taken.

7 Conclusions

In this chapter, a new Dynamic Data-Driven Application System (DDDAS) is demonstrated that allows the quantification and measurement of uncertainties in experimental data, model parameters, and in the selection of the model itself for monitoring and controlling damage in composite materials such as are common in

aircraft structures. In this regard, uniaxial tensile experiments with different load levels and including loading-unloading cycles are conducted on laboratory manufactured carbon nanotube infused epoxy nanocomposites. In order to provide information for real-time monitoring of damage, the spatial variation in the strain field over time is measured using digital image correlation. Computational models based on continuum damage mechanics is considered to characterize the progressive damage and degradation in the material. Among the various existing evolution equations for damage that are available in the literature, two damage models (Krajcinovic and Marigo) are picked for the statistical calibration, model ranking, and real-time monitoring of damage. Moreover, a Bayesian framework for uncertainty quantification, calibration, validation, and selection of models is described in this work. Since the damage growth in the material depends on the underlying dynamics at the micro-scale over time (evolution of micro-crack, micro-voids, etc), Bayesian filtering is used in this study, enabling the damage models to adjust to the new experimental data and update the damage state in real-time.

To implement the DDDAS, an integrated infrastructure, expressed in software, is developed to incorporate: the numerical algorithms for a finite element solution of the continuum damage models; generated experimental data; algorithms for sampling as well as model calibration, plausibility, and selection based on Bayesian-based methods; and Bayesian filtering procedure.

The constructed DDDAS enables real time statistical calibration of classes of computational models of material damage, while accounting fo uncertainties in parameters and data. The system employs Bayesian filters for real time monitoring of the evolution of damage that enables forecasting the location of the local material degradation that can lead to system failure. A new feature of control made possible by the Bayesian framework is the calculation of model plausibilities to allow the dynamic selection of the damage model that best fits current experimental data.

In summary, the development of a successful DDDAS infrastructure compiles a diverse range of technologies, including precise experimental techniques, micromechanical evolution models of the damage and pre-failure of materials, Bayesian inference, information theory, parallel sampling algorithms, and high performance computing. The outcomes suggest that not only is this a feasible approach, but that it defines a powerful new technology for developing predictive models of complex physical phenomena.

Acknowledgements The research in this chapter was supported under AFOSR contract FA9550-11-1-0314. The authors acknowledge the important support of DDDAS research by Dr. Frederica Darema of AFOSR. The authors would like to thank Drs. P. T. Bauman and E. E. Prudencio for developing the software and conducting the computational work, and Mr. S. V. Williams for assistance in performing the experimental work.

References

1. F. Darema, DDDAS: Dynamic Data Driven Applications Systems, http: //www.nsf.gov /cise /cns /dddas.
2. F. Darema, Dynamic Data Driven Applications Systems: A New Paradigm for Application Simulations and Measurements, Vol. 3038 of Lecture Notes in Computer Science, Springer, 2004.
3. F. Darema, Dynamic data driven applications systems: A new paradigm for application simulations and measurements, in: M. Bubak, G. D. v. Albada, P. M. A. Sloot, J. J. Dongarra (Eds.), Computational Science - ICCS 2004, Vol. 3038 of Lecture Notes in Computer Science, Springer Berlin / Heidelberg, 2004, pp. 662–669.
4. F. Darema, Grid computing and beyond: The context of dynamic data driven applications systems, Proceedings of the IEEE 93 (3) (2005) 692–697.
5. F. Darema, Characterizing dynamic data driven applications systems (dddas) in terms of a computational model, in: G. Allen, J. Nabrzyski, E. Seidel, G. van Albada, J. Dongarra, P. Sloot (Eds.), Computational Science ICCS 2009, Vol. 5545 of Lecture Notes in Computer Science, Springer Berlin / Heidelberg, 2009, pp. 447–448.
6. F. Darema, M. Rotea, Dynamic data-driven applications systems, in: Proceedings of the 2006 ACM/IEEE conference on Supercomputing, SC '06, ACM, New York, NY, USA, 2006.
7. F. Darema, H. E. Seidel, Report of the August 2010 Multi-Agency Workshop on InfoSymbiotic/DDDAS. The Power of Dynamic Data Driven Applications Systems (2011).
8. L. M. Kachanov, On time to rupture in creep conditions, Izviestia Akademii Nauk SSSR 8 (1958) 26–31.
9. J. Lemaitre, J. L. Chaboche, Mechanics of Solid Materials, Combridge University Press, 1990.
10. E. E. Prudencio, P. T. Bauman, S. V. Williams, D. Faghihi, K. Ravi-Chandar, J. T. Oden, Real-time inference of stochastic damage in composite materials, International Journal of Solid and Structure (in review).
11. D. Krajcinovic, G. U. Fonseka, The continuous damage theory of brittle materials, Parts 1 and 2, Journal of Applied Mechanics 48 (1981) 809–824.
12. J. J. Marigo, Formulation of a damage law for elastic material, Count-returned of Acadmie of Sciences. Paris, Srie II 292 (1981) 13091312.
13. G. Belloni, G. Bernasconi, G. Piatti, Creep Damage Models. In: Creep of Engineering Materials and Structures, Applied Science Publisher, 1979.
14. E. T. Jaynes, Probability Theory: The Logic of Science, Cambridge University Press, 2003.
15. S. H. Cheung, T. A. Oliver, E. E. Prudencio, S. Prudhomme, R. D. Moser, Bayesian uncertainty analysis with applications to turbulence modeling, Reliability Engineering and System Safety 96 (2011) 1137–1149.
16. E. E. Prudencio, S. H. Cheung, Parallel adaptive multilevel sampling algorithms for the Bayesian analysis of mathematical models, International Journal for Uncertainty Quantification 2 (3) (2012) 215–237.
17. J. T. Oden, E. E. Prudencio, A. Hawkins-Daarud, Selection and assessment of phenomenological models of tumor growth, Mathematical Models and Methods in Applied Sciences.
18. A. M. Fraser, Hidden Markov Models and Dynamical Systems, SIAM, 2008.
19. A. H. Jazwinski, Stochastic Processes and Filtering Theory, Dover, 1998.
20. G. Welch, G. Bishop, An Introduction to the Kalman Filter, http://www.cs.unc.edu / welch/ kalman/ kalmanIntro.html, uNC-Chapel Hill TR 95-041 (2006).
21. E. E. Prudencio, P. T. Bauman, D. Faghihi, K. Ravi-Chandar, J. T. Oden, Bayesian model selection in data driven analyses of material damage, International Journal for Numerical Methods in Engineering (in review).